



Predicting Ductile Fracture in Maritime Crash with a Modified Implementation of BWH Criterion

Burak Can Cerik^(✉), Sung-Ju Park, and Joonmo Choung

Department of Naval Architecture and Ocean Engineering, Inha University,
Incheon, Republic of Korea
bccerik@inha.ac.kr

Abstract. This paper presents a modified numerical implementation of the BWH (Bressan-Williams-Hill) criterion for predicting ductile fracture in non-linear finite element analysis of steel-plated structures with shell elements. The original BWH criterion is transformed to the equivalent plastic strain-stress triaxiality space and considered as the failure envelope under proportional loading. A linear damage evolution law is used, which expresses the necking indicator as equivalent plastic strain increment weighted with the localized necking envelope under proportional loading. The bending induced suppression of localized necking is considered by tracing the evolution of the necking indicator in all through-thickness integration points separately. The BWH criterion with the proposed modifications is implemented in a user-defined VUMAT subroutine and applied in the simulations of various stretch-bending and stiffened panel penetration tests reported in the literature. It is demonstrated that the proposed implementation of the BWH criterion provides a better estimate of displacement to fracture initiation.

Keywords: Ductile fracture · Collision and grounding · Shell element

1 Introduction

In an accidental over-loading scenario, such as collision or stranding, the structural member of a ship most prone to rupture, the outer shell plating, will fail under dominantly biaxial stretching loading. In most cases, with a possible exception of equi-biaxial tension, where shear banding may occur, the failure mechanism of steel-plated structures plates under biaxial stretching is strain localization in form of a neck and subsequent fracture. A pragmatic approach for modeling ductile fracture in such scenarios with large shell finite elements having an element size that is several multiples of the plate thickness, is to assume the onset of localized necking as the failure condition and ignore the post-necking response, which cannot be modeled with shell elements due to plane stress assumption and size effects. A forming limit curve (FLC) is commonly used in sheet metal forming industry for the prediction of the onset of

localized necking. As demonstrated by Zhu and Atkins about two decades ago [22], this concept may be utilized for ship collision and grounding analysis as well. A well-known localized necking criterion by the maritime crash community, Bressan-Williams-Hill (BWH) criterion, which was introduced by Alsos et al. [2], is re-visited in the present paper to address two known issues of FLCs: loading path effect and bending induced suppression of localized necking.

The most serious drawback of FLCs is probably their loading-path dependency, which means that the limit curve is non-unique under complex loading histories or non-proportional loading conditions. The FLC is constructed either by conducting tests leading almost proportional loading paths (stress state characterized usually by a constant principal strain ratio), or using analytical formulations, such as Hill [10], Stören-Rice [19] or Marciniak-Kuczyński (MK) [14] models that assume proportional stretching of sheet metals. However, in practical cases, such as metal forming as well as crash, the loading paths can be strongly non-proportional [15]. In such cases, the FLCs are, therefore, incapable of predicting the onset of localized necking correctly. As advocated by Stoughton [21], a stress-based FLC (expressed in the principal stress space rather than principal strain space) is less loading path-dependent. Indeed, the original BWH criterion is also a stress-based necking criterion. In path-independent FLC formulations, regardless of the variable space in which the FLC is expressed, only the final state of stress that is of any concern and the histories of strain and stress are insignificant. Alternatively, a necking indicator, which accumulates with equivalent plastic increment weighted with the localized necking locus function [4], may be utilized for considering entire loading history [11].

During large deformation of steel-plated structures, like ship hull structures during collision, both large curvature bending and stretching may take place [9]. The FLCs are valid only for membrane stretching and do not include bending effects. In the numerical implementation of FLCs, usually the failure of the mid-layer through-thickness integration point of the shell element is checked, so that failure only due to membrane deformation is considered. Seong et al. [18] demonstrated that the bending deformation delays or even suppresses localized necking. Previous extensions of BWH criterion [20] focused on treatment of post-necking response, which is omitted in the original BWH criterion and attributed to be the source of conservative failure prediction. However, no attention was given on the bending-induced delay of incipient localized necking, which may be a more serious drawback of the original BWH criterion as compared to the omission of post-necking response. To deal with the bending-induced suppression of localized necking, the necking indicator accumulation in individual thickness integration points may be considered separately [7, 13, 16].

Against this background, the objective of this study is to modify the implementation of the BWH criterion by inclusion of loading path effect through a necking indicator framework and consideration of through-thickness strain gradients. A user-defined material subroutine is developed implementing the proposed modifications, and applied on the simulations of stretch-bending tests of a shipbuilding steel and penetration tests of stiffened panels.

2 Modeling of Plasticity and Fracture Initiation

2.1 Plasticity

In this paper, all materials are assumed to obey von Mises yield condition, associative flow rule and isotropic strain hardening. In addition, plane stress condition holds, i.e. the third principal stress, σ_3 , is zero. The isotropic von Mises yield condition is given by

$$f[\boldsymbol{\sigma}, k] = \bar{\sigma} - k = 0 \quad (1)$$

where k is the deformation resistance and $\bar{\sigma}$ is the von Mises equivalent stress under plane stress condition, which is expressed in terms of principal stresses (σ_1, σ_2) as follows:

$$\bar{\sigma} = \sqrt{\sigma_1^2 + \sigma_2^2 - \sigma_1\sigma_2} \quad (2)$$

The plastic strain increments, $d\boldsymbol{\varepsilon}_p$ are derived from an associative flow rule, where the plastic potential is equal to the yield surface function, $\bar{\sigma}$:

$$d\boldsymbol{\varepsilon}_p = (d\bar{\varepsilon}_p) \frac{\partial \bar{\sigma}}{\partial \boldsymbol{\sigma}} \quad (3)$$

The equivalent plastic strain increment, $d\bar{\varepsilon}_p$, is defined as the work-conjugate of the von Mises equivalent stress:

$$\boldsymbol{\sigma} : d\boldsymbol{\varepsilon}_p = \bar{\sigma} d\bar{\varepsilon}_p \quad (4)$$

Ignoring rate- and temperature-dependency, the deformation resistance, k , is a monotonic function of the equivalent plastic strain, i.e. a strain hardening function:

$$k = f[\bar{\varepsilon}_p] \quad (5)$$

In practice, a power law, such as Swift law given below, is appropriate to describe the irreversible evolution of the flow stress of marine structural steels:

$$k[\bar{\varepsilon}_p] = \begin{cases} \sigma_0 & \text{if } \bar{\varepsilon}_p \leq \bar{\varepsilon}_L \\ K(\varepsilon_0 + \bar{\varepsilon}_p)^n & \text{if } \bar{\varepsilon}_p > \bar{\varepsilon}_L \end{cases} \quad (6)$$

where σ_0 is the initial flow stress, $\bar{\varepsilon}_L$ is Lüders plateau strain, K , n and ε_0 are the Swift law parameters.

2.2 Bressan-Williams and Hill Localized Necking Criteria

The ratio of principal plastic strains, α , is defined as below, and assumed to remain constant (proportional loading):

$$\alpha = \frac{\varepsilon_2}{\varepsilon_1} \quad (7)$$

The BWH criterion, as proposed by Alsos et al. [2], is a combination of Hill’s localized necking criterion [10], which is valid in the range bordered by the uniaxial tension ($\alpha = -0.5$) and plane strain tension ($\alpha = 0$) stress states, and Bressan and Williams’ shear instability-based localized necking criterion [5], which is used for the range bordered by the plane strain tension and equi(balanced)-biaxial tension ($\alpha = 1$) stress states. The criterion is expressed in the principal stress-principal strain ratio space as follows:

$$\sigma_{1,n}[\alpha] = \begin{cases} \frac{2K}{\sqrt{3}} \frac{1+0.5\alpha}{\sqrt{1+\alpha+\alpha^2}} \left(\frac{2}{\sqrt{3}} \frac{\hat{\epsilon}_1}{1+\alpha} \sqrt{1+\alpha+\alpha^2} \right)^n, & \text{for } -0.5 \leq \alpha \leq 0 \\ \frac{2K}{\sqrt{3}} \frac{\left(\frac{2}{\sqrt{3}} \hat{\epsilon}_1 \right)^n}{\sqrt{1-\left(\frac{\alpha}{2+\alpha}\right)^2}}, & \text{for } 0 \leq \alpha \leq 1 \end{cases} \quad (8)$$

where $\hat{\epsilon}_1$ is major necking strain corresponding to the plain strain tension state ($\alpha = 0$). Using a power-law hardening function (Holloman type), it may be assumed as the hardening exponent n . Note that in the above equation, K and n are the power law hardening parameters.

Note that the applicability range of the Hill’s criterion is corrected in the present paper, which, in the original formulation by Alsos et al. [2], was given as $-1.0 \leq \alpha \leq 0$, covering shear dominated stress states. In addition, the upper range for Bressan-Williams criterion is set as the equi-biaxial tension state.

2.3 Transformation to Different Variable Spaces

The BWH criterion is transformed to the space of equivalent plastic strain-stress triaxiality, which is easier to interpret for the ship collision and grounding community. Prior to introducing the transformations, it would be useful to define the principal stress ratio, β , and stress triaxiality, η :

$$\beta = \frac{\sigma_2}{\sigma_1} \quad (9)$$

$$\eta = \frac{\sigma_m}{\bar{\sigma}} = \frac{\sigma_1 + \sigma_2}{3\bar{\sigma}} \quad (10)$$

where $\sigma_m/3$ is the mean stress. Note that $\sigma_3 = 0$.

The derivations for the transformation formulas were provided by Lee [12]. Under the assumptions provided in the plasticity model description, for proportional loading paths, a relation exists between α and β :

$$\alpha = \frac{2\beta - 1}{2 - \beta} \quad (11)$$

$$\beta = \frac{2\alpha + 1}{2 + \alpha} \quad (12)$$

The stress triaxiality can be expressed in terms of α and β as follows:

$$\eta = \frac{\alpha + 1}{\sqrt{3(\alpha^2 + \alpha + 1)}} = \frac{\beta + 1}{3\sqrt{\beta^2 - \beta + 1}} \quad (13)$$

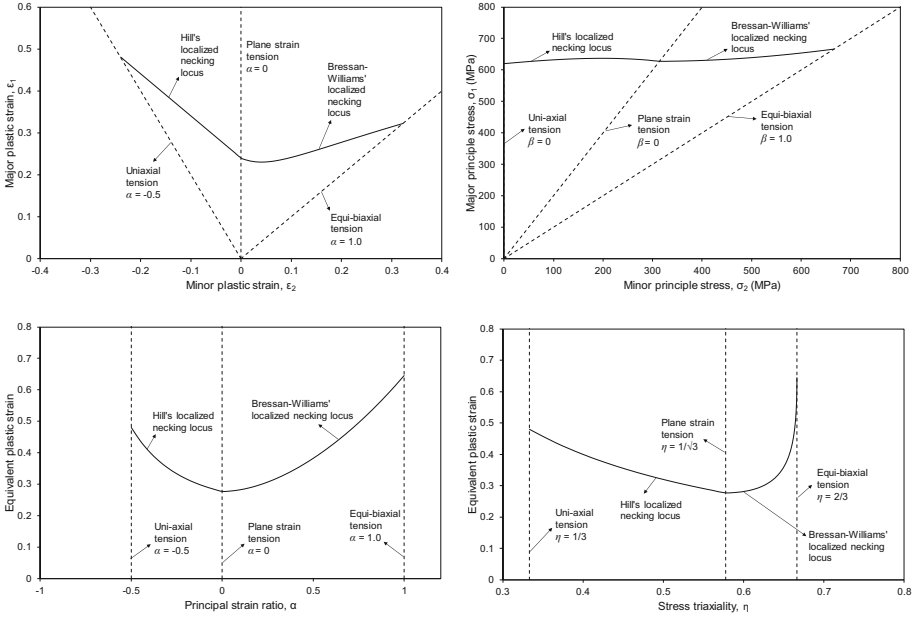


Fig. 1. Localized necking locus of grade S235JR steel plotted in different variable spaces

The equivalent plastic strain is expressed in terms of α and ε_1 as follows:

$$\bar{\varepsilon}_p = \frac{2\varepsilon_1}{\sqrt{3}} \sqrt{1 + \alpha + \alpha^2} \quad (14)$$

Lastly, the equivalent von Mises stress may be transformed to σ_1 as follows:

$$\sigma_1 = \frac{\bar{\sigma}}{\sqrt{1 - \beta + \beta^2}} \quad (15)$$

Using the above equations and the hardening law to relate equivalent plastic strain to equivalent stress, it will be straightforward to transform the BWH criterion can be transformed to the spaces of (σ_1, σ_2) , $(\bar{\varepsilon}_p, \alpha)$, $(\bar{\varepsilon}_p, \eta)$ and $(\bar{\varepsilon}_p, \eta)$. Figure 1 shows the localized necking locus of grade S235JR steel plotted using the hardening function parameters provided in [1].

2.4 Treatment of Loading Path and Bending Effects

For non-proportional loading paths, the necking indicator, N , is introduced [4]. The necking indicator accumulates with the equivalent plastic increment, which is weighted with the localized necking locus function that is strictly valid for proportional loading, $\bar{\varepsilon}_n[\eta]$, and expressed in the space of $(\bar{\varepsilon}_p, \eta)$:

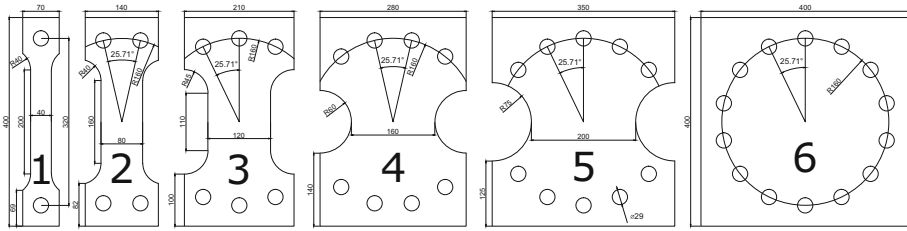


Fig. 2. Dimensions of the formability test specimens (unit: mm)

$$dN = \frac{d\bar{\epsilon}_p}{\bar{\epsilon}_n [\eta]} \tag{16}$$

For shell finite elements, the evolution of the necking indicator, N , is considered in individual thickness integration points separately. To distinguish membrane and bending loads, and take into account bending induced suppression of localized necking, failure of all through-thickness integration points is assumed to occur only if the necking indicator reaches unity for all through-thickness integration points:

$$N[z] = 1 \quad \forall z \in [-t/2, t/2] \tag{17}$$

where t is the shell element thickness. In other words, even though the failure condition ($N = 1$) may be satisfied at an individual through-thickness integration point, the stress tensor components for that particular integration point are not set to zero (i.e. $\sigma = 0$), unless all other through-thickness integration points meet the necking condition. The described model is implemented to Abaqus/Explicit through a user defined material subroutine VUMAT.

3 Formability Tests

First, the formability tests with 12 mm thick specimens made of shipbuilding mild steel, reported in [6], were simulated with the developed fracture model. The tests include six different specimen geometries, which are shown in Fig. 2. The specimens were clamped outside a radius of 140 mm, and loaded with an indenter having a spherical tip with a 60 mm diameter. Hence, the tests can be considered as stretch-bending testing of relatively thick plates as compared to sheet metals used in the forming industry.

The finite element solver Abaqus/Explicit was used for simulating the tests with shell elements and the developed VUMAT subroutine. Four node shell elements with reduced integration (S4R) were employed. Five through-thickness integration points were used, which were deemed to appropriate to account for bending effects. A nominal element size of 9.6 mm (0.8 times of the plate thickness) was selected to achieve sufficient resolution of strains and allow direct comparison with the simulation results reported in [20], where the original and a different extension of BWH criterion was used. Figure 3 shows the mesh configuration of all specimens. It should be noted that the use of a necking criterion

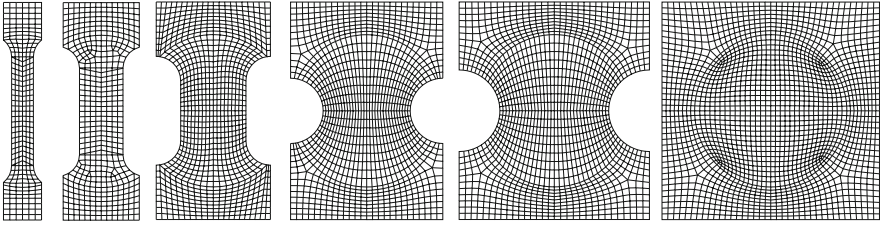


Fig. 3. Mesh configuration of formability test specimens

as a failure criterion makes the implicit assumption that the elements are so much larger than the neck so that the elongation due to necking after the onset of necking can be neglected. The used mesh size somehow violates this assumption, however, the geometry of the specimens, particularly the first two, requires a mesh size that is in the order of plate thickness to capture strain gradients accurately. The hardening law parameters and the coefficient of friction between the contacting surfaces were taken from [20]. Both in-plane and out-of-plane constraints were assumed for the clamped sections of the test specimens, without modeling the bolt holes.

Figure 4 compares the force-displacement curves from the formability tests and the FE simulations. It is evident that the instants of sudden drop of the force in all tests, which corresponds to ductile fracture initiation, were captured well in the FE simulations. Slight deviations for the force levels at large displacements, particularly in the results of specimens 4–6, were apparently due to assumed boundary conditions that could not reflect the actual constraints in the tests very closely. As compared to the predictions with the proposed extension of the BWH criterion, the original BWH criterion, as reported in [20], predicts the failure earlier. The difference is particularly large for the specimens 2, 3, 4, and 5. The differences may be attributed to the bending-induced suppression of localized necking, which is not considered in the original BWH criterion.

4 Stiffened Panel Indentation Tests

The panel indentation test by Alsos and Amdahl [1] were re-visited with the proposed extension of BWH criterion to gain more insights at structural level. Three test model geometries were adopted by Alsos and Amdahl [1]: an unstiffened panel (US), a panel with a flat-bat stiffener (FB-1) at the center and a panel with two flat-bar stiffeners (FB-2). The panels were 1200×720 mm and made of 5 mm thick S235JR grade mild steel, whereas the flat-bar stiffeners were 6 mm thick and made of the same steel grade but with different hardening properties. The test models were welded to a 12 mm thick box frame and indented with conical indenter with spherical nose of 200 mm radius.

In the numerical modeling of the tests, three different mesh sizes, namely $5t$, $4t$ and $3t$ were considered to assess the sensitivity of the failure modeling to

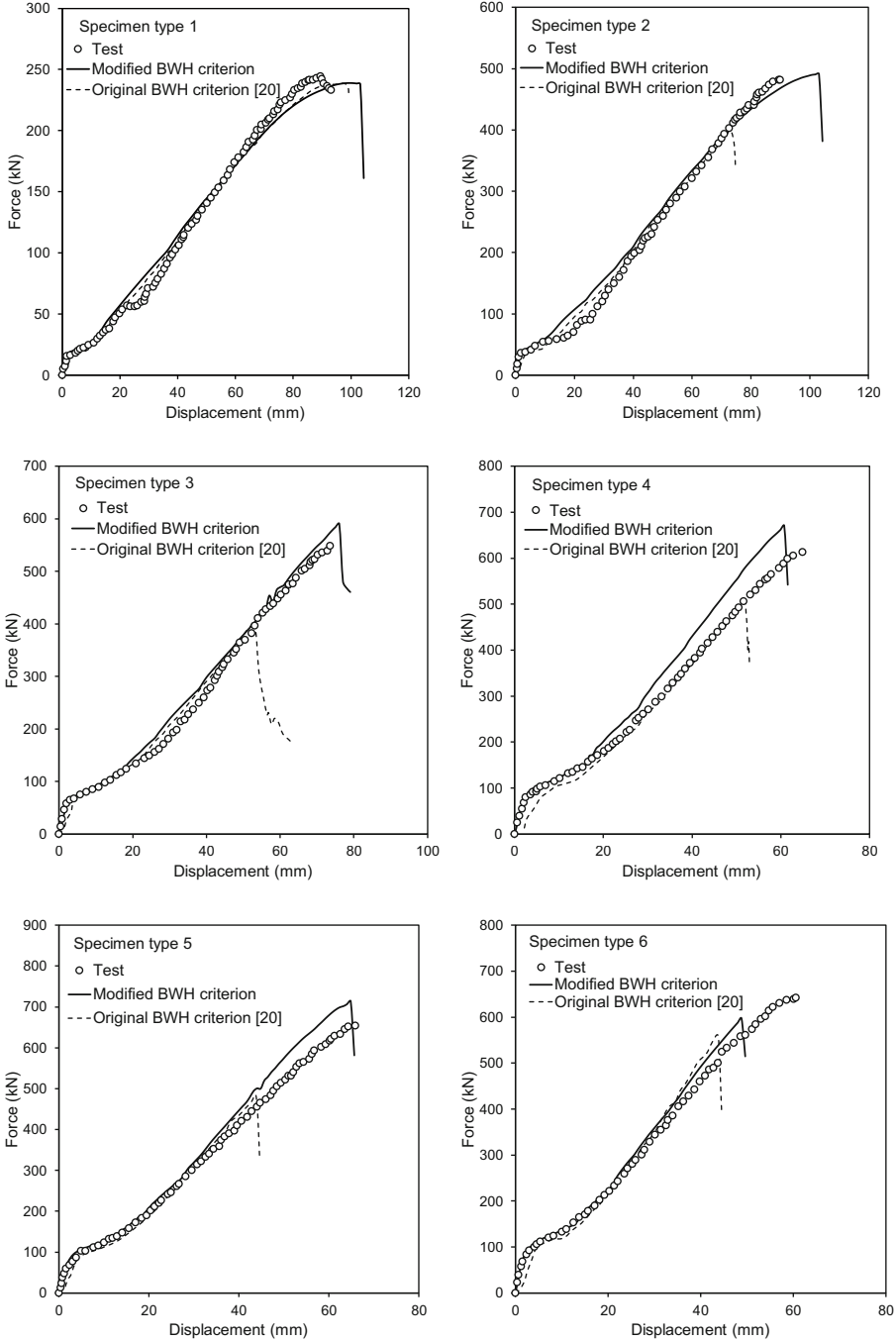


Fig. 4. Force-displacement curves from the formability tests and FE simulations

discretization, where t is the plate thickness. The same element type as in the formability test simulations was used. Again, the hardening law parameters and the friction coefficient were same as those given in [20]. The strong box frame was not included in the FE models and fixed boundary conditions were assumed, where the test models were welded to the frame. The effect of this idealization was found to be negligible. As contrary to [20], the weld intersections between the based plate and stiffeners were not modeled with elements having increased thickness.

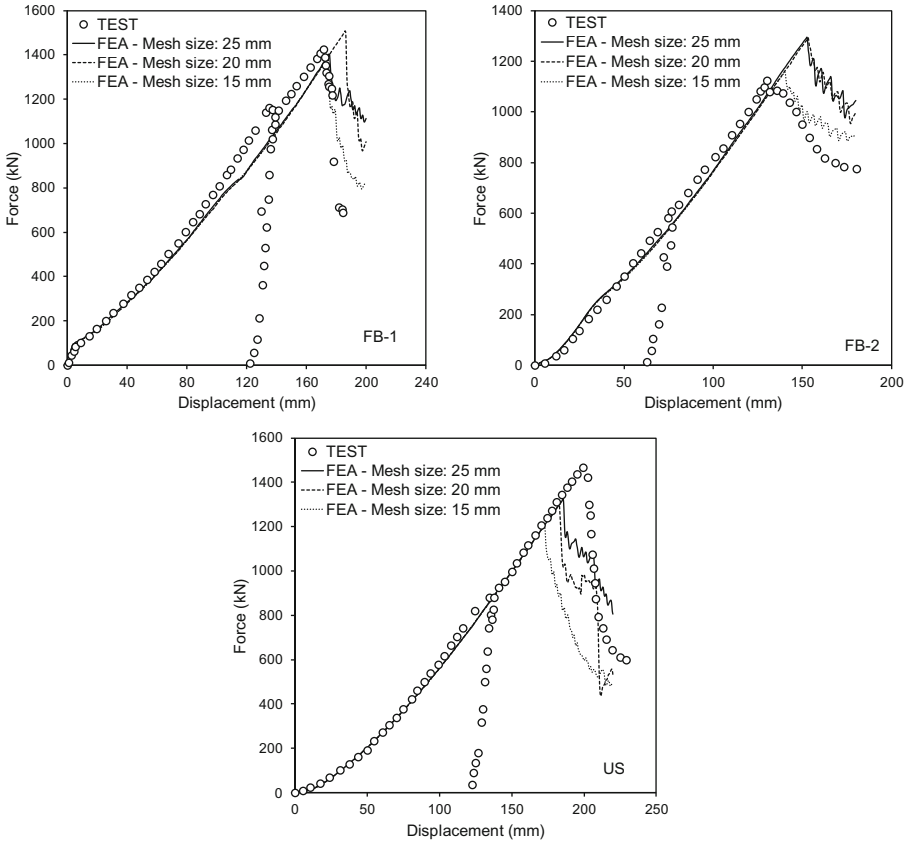


Fig. 5. Force-displacement curves from the panel indentation tests and FE simulations

A comparison of the test results and the FE simulations with different mesh sizes are shown in Fig. 5. It is evident that the enhanced BWH criterion predicts the onset of fracture initiation accurately, without employing any regularization of fracture criterion based on mesh size or damage induced softening model after the onset of localized necking. Figure 6 shows a comparison between the original

BWH criterion and the modified one proposed in the present work for the case of 15 mm mesh size. Contrary to the formability tests, the differences are marginal. This can be explained with the fact that membrane stretching is dominant in the panel penetration tests with a large indenting surface.

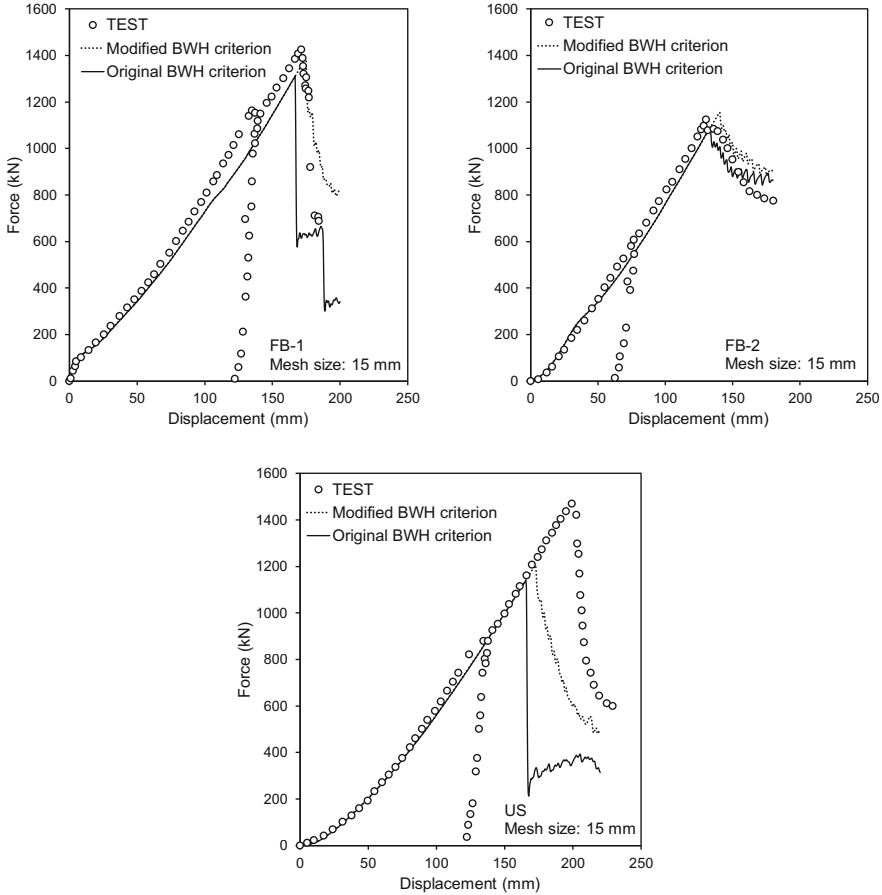


Fig. 6. Force-displacement curves from the panel indentation tests and FE simulations

It should be noted that in the simulations of FB-1 and FB-2, the predicted location of the fracture initiation was on the face plate, close to the stiffener but not exactly on the plate-stiffener interaction, as shown in Figs. 7 and 8, where the contours show the necking indicator, N . This prediction is correct for FB-2, however, not for FB-1. Nevertheless, for both models, the global behavior as reflected in the force-displacement response followed closely in the simulations.

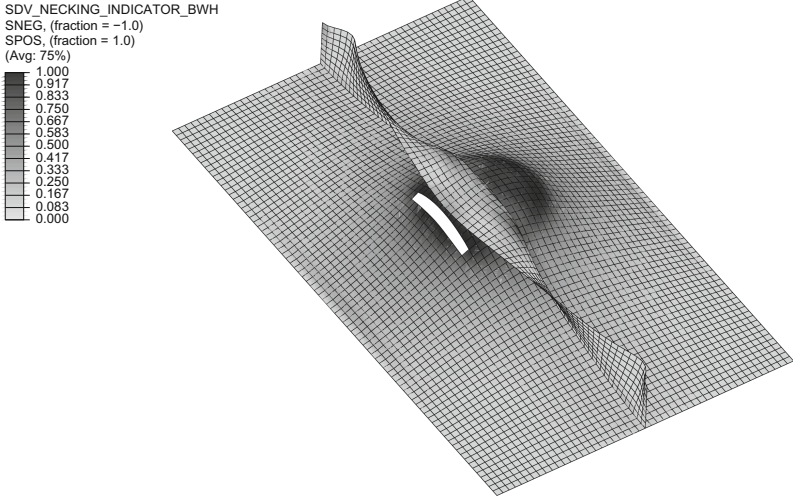


Fig. 7. Post-fracture shape of FB-1 (mesh size: 15 mm)

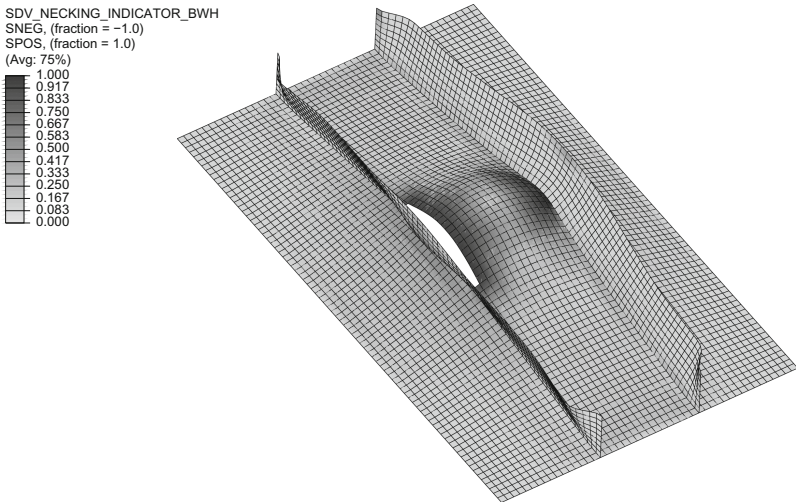


Fig. 8. Post-fracture shape of FB-2 (mesh size: 15 mm)

Figure 9 shows the loading paths and necking indicator evolution in top and bottom through-thickness integration points of the first deleted elements in the simulations of US, FB-1 and FB-2. Here, bottom surface denotes the surface in contact with the indenter. In case of US and FB-1, the top surfaces are exhibit almost proportional loading paths, which are close to equi-biaxial stress state. The bottom surfaces, on the other hand, experience non-proportionality. In the case of FB-2, the bottom surface is almost in plane-strain tension state

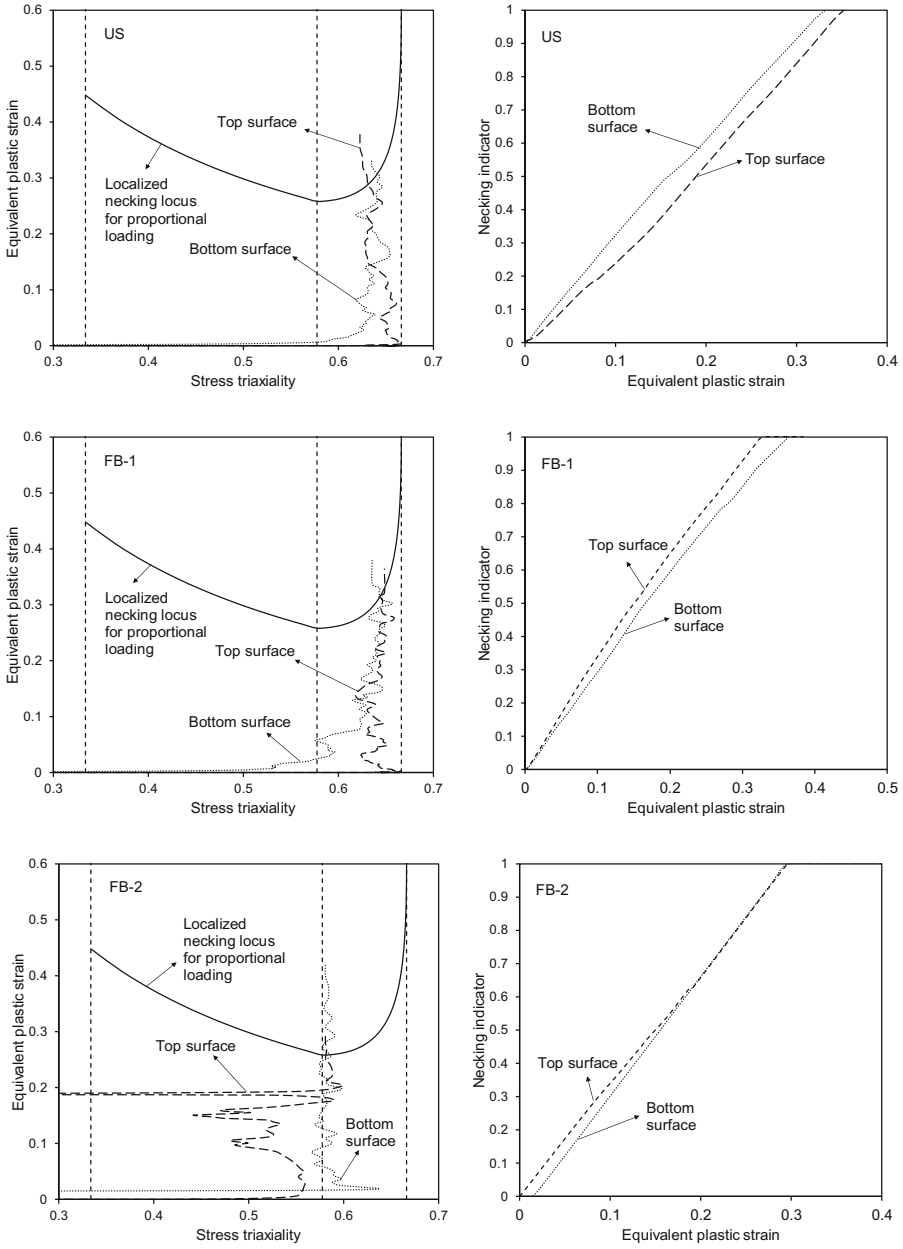


Fig. 9. Loading paths and necking indicator evolution in top and bottom through-thickness integration points of the first deleted elements

throughout the loading until element removal, whereas the top surface goes through different stress states. The evolution of necking indicators, which are shown on the right hand side of Fig. 9, demonstrates clearly that the effect of bending deformation is slight, and for the case of FB-2, it is negligible. The necking indicator evolutions for top and bottom surfaces are different due to experiencing different loading paths.

The BWH criterion deals with fracture preceded by localized necking. There are other failure mechanisms (see [3]), such as in-plane shear fracture, surface cracking due to bending and wrinkling, which occur without the occurrence of necking. A complete failure model for shell finite elements require not only necking based failure modeling but also pragmatic methods for handling other failure mechanisms. Future studies should address the likelihood of the other failure mechanisms in maritime crash analysis and whether in marine structural steel plates fracture can occur under biaxial stretching before necking.

5 Concluding Remarks

In the present work, the BWH criterion was modified to deal with non-proportional loading paths within a damage indicator framework and to consider bending induced suppression of localized necking. The same set of experiments as in [20] to demonstrate the enhancements achieved with the proposed modifications. It was shown that the proposed model performs better particularly for the cases where membrane stretching does not dominate the response fully and bending deformation take place initially. Further work should consider validating the proposed model with larger test models, preferably made of high tensile steel used in the actual ship structures [8, 17].

Acknowledgements. This work was supported by Korea Research Fellowship Program through the National Research Foundation of Korea (NRF) funded by the Ministry of Science and ICT (2017H1D3A1A01055137).

References

1. Alsos, H.S., Amdahl, J.: On the resistance to penetration of stiffened plates, part I-experiments. *Int. J. Impact Eng.* **36**, 799–807 (2009). <https://doi.org/10.1016/j.ijimpeng.2008.10.005>
2. Alsos, H.S., Hopperstad, O.S., Törnqvist, R., Amdahl, J.: Analytical and numerical analysis of sheet metal instability using a stress based criterion. *Int. J. Solids Struct.* **45**, 2042–2055 (2008). <https://doi.org/10.1016/j.ijsolstr.2007.11.015>
3. Atli-Veltin, B., Walters, C.L., Dekker, R., Brunner, S.K.: Wrinkling, fracture, and necking: the various failure modes in maritime crash. In: *Proceedings of the 35th International Conference on Ocean, Offshore and Arctic Engineering, OMAE2016*, Busan, Korea pp. V003T02A005. ASME (2016). <https://doi.org/10.1115/OMAE2016-54148>
4. Bai, Y., Wierzbicki, T.: Forming severity concept for predicting sheet necking under complex loading histories. *Int. J. Mech. Sci.* **50**, 1012–1022 (2008). <https://doi.org/10.1016/j.ijmecsci.2008.02.010>

5. Bressan, J.D., Williams, J.A.: The use of a shear instability criterion to predict local necking in sheet metal deformation. *Int. J. Mech. Sci.* **25**, 155–168 (1983). [https://doi.org/10.1016/0020-7403\(83\)90089-9](https://doi.org/10.1016/0020-7403(83)90089-9)
6. Broekhuijsen, J.: Ductile failure and energy absorption of Y-shape test section. Master thesis, Delft University of Technology, Delft, the Netherlands (2003)
7. Cerik, B.C., Lee, K., Park, S.-J., Choung, J.: Simulation of ship collision and grounding damage using Hosford-Coulomb fracture model for shell elements. *Ocean Eng.* **173**, 415–432 (2019). <https://doi.org/10.1016/j.oceaneng.2019.01.004>
8. Cerik, B.C., Park, B., Park, S.-J., Choung, J.: Modeling, testing and calibration of ductile crack formation in grade DH36 ship plates. *Mar. Struct.* **66**, 27–43 (2019). <https://doi.org/10.1016/j.marstruc.2019.03.003>
9. Costas, M., Morin, D., Hopperstad, O.S., Børvik, T., Langseth, M.: A through-thickness damage regularisation scheme for shell elements subjected to severe bending and membrane deformations. *J. Mech. Phys. Solids* **123**, 190–206 (2019). <https://doi.org/10.1016/j.jmps.2018.08.002>
10. Hill, R.: On discontinuous plastic states, with special reference to localized necking in thin sheets. *J. Mech. Phys. Solids* **1**, 19–30 (1952). [https://doi.org/10.1016/0022-5096\(52\)90003-3](https://doi.org/10.1016/0022-5096(52)90003-3)
11. Körgesaar, M.: The effect of low stress triaxialities and deformation paths on ductile fracture simulations of large shell structures. *Mar. Struct.* **63**, 45–64 (2019). <https://doi.org/10.1016/j.marstruc.2018.08.004>
12. Lee, Y-W.: Fracture prediction in metal sheets. Ph.D. dissertation, Massachusetts Institute of Technology, Cambridge, MA (2007)
13. Li, Y., Luo, M., Gerlach, J., Wierzbicki, T.: Prediction of shear-induced fracture in sheet metal forming. *J. Mater. Process. Technol.* **210**, 1858–1869 (2010). <https://doi.org/10.1016/j.jmatprotec.2010.06.021>
14. Marciniak, Z., Kuczyński, K.: Limit strains in the processes of stretch-forming sheet metal. *Int. J. Mech. Sci.* **9**, 609–620 (1967). [https://doi.org/10.1016/0020-7403\(67\)90066-5](https://doi.org/10.1016/0020-7403(67)90066-5)
15. Mattiasson, K., Jergéus, J., DuBois, P.: On the prediction of failure in metal sheets with special reference to strain path dependence. *Int. J. Mech. Sci.* **88**, 175–191 (2014). <https://doi.org/10.1016/j.ijmecsci.2014.08.006>
16. Pack, K., Mohr, D.: Combined necking & fracture model to predict ductile failure with shell finite elements. *Eng. Fract. Mech.* **182**, 32–51 (2017). <https://doi.org/10.1016/j.engfracmech.2017.06.025>
17. Park, S.-J., Lee, K., Cerik, B.C., Choung, J.: Ductile fracture prediction of EH36 grade steel based on Hosford-Coulomb models. *Ships Offshore Struct.* (2019). <https://doi.org/10.1080/17445302.2019.1565300>
18. Seong, D.Y., Haque, M.Z., Kim, J.B., Stoughton, T.B., Yoon, J.W.: Suppression of necking in incremental sheet forming. *Int. J. Solids Struct.* **51**, 2840–2849 (2014). <https://doi.org/10.1016/j.ijsolstr.2014.04.007>
19. Stören, S., Rice, J.R.: Localized necking in thin sheets. *J. Mech. Phys. Solids* **6**, 421–441 (1975). [https://doi.org/10.1016/0022-5096\(75\)90004-6](https://doi.org/10.1016/0022-5096(75)90004-6)
20. Storheim, M., Alsos, H.S., Hopperstad, O.S., Amdahl, J.: A damage-based failure model for coarsely meshed shell structures. *Int. J. Impact Eng.* **83**, 59–75 (2015). <https://doi.org/10.1016/j.ijimpeng.2015.04.009>
21. Stoughton, T.B.: Stress-based forming limits in sheet-metal forming. *J. Eng. Mater. Technol.* **123**, 417–422 (2001). <https://doi.org/10.1115/1.1398083>
22. Zhu, L., Atkins, A.G.: Failure criteria for ship collision and grounding. In: 7th International Symposium on Practical Design of Ships and Mobile Units, PRADS' 1998, New York, pp. 149–156. Elsevier (1998)